2024

Gamma Amplitude-Envelope Correlations Are Strongly Elevated within Hyperexcitable Networks in Focal Epilepsy

Manoj Raghavan
Medical College of Wisconsin

Jared Pilet
Marquette University

Chad Carlson
Medical College of Wisconsin

Christopher T. Anderson
Medical College of Wisconsin

Wade Mueller
Medical College of Wisconsin

See next page for additional authors

scientific reports

Check for updates

OPEN

Gamma amplitude-envelope correlations are strongly elevated within hyperexcitable networks in focal epilepsy

Manoj Raghavan[1]✉, Jared Pilet[3], Chad Carlson[1], Christopher T. Anderson[1], Wade Mueller[2], Sean Lew[2], Candida Ustine[1], Priyanka Shah-Basak[1], Vahab Youssofzadeh[1] & Scott A. Beardsley[3]

Methods to quantify cortical hyperexcitability are of enormous interest for mapping epileptic networks in patients with focal epilepsy. We hypothesize that, in the resting state, cortical hyperexcitability increases firing-rate correlations between neuronal populations within seizure onset zones (SOZs). This hypothesis predicts that in the gamma frequency band (40–200 Hz), amplitude envelope correlations (AECs), a relatively straightforward measure of functional connectivity, should be elevated within SOZs compared to other areas. To test this prediction, we analyzed archived samples of interictal electrocorticographic (ECoG) signals recorded from patients who became seizure-free after surgery targeting SOZs identified by multiday intracranial recordings. We show that in the gamma band, AECs between nodes within SOZs are markedly elevated relative to those elsewhere. AEC-based node strength, eigencentrality, and clustering coefficient are also robustly increased within the SOZ with maxima in the low-gamma band (permutation test Z-scores > 8) and yield moderate discriminability of the SOZ using ROC analysis (maximal mean AUC ~ 0.73). By contrast to AECs, phase locking values (PLVs), a measure of narrow-band phase coupling across sites, and PLV-based graph metrics discriminate the seizure onset nodes weakly. Our results suggest that gamma band AECs may provide a clinically useful marker of cortical hyperexcitability in focal epilepsy.

Keywords Focal epilepsy, Cortical hyperexcitability, Electrocorticography, Functional connectivity, Gamma amplitude envelope correlations, Seizure onset zones

Epilepsy is a neurological disorder characterized by hyperexcitable brain networks that give rise to recurrent seizures[1]. About one-third of patients with epilepsy fail to achieve satisfactory seizure control with anti-seizure medications alone[2]. A subset of these patients may benefit from surgery to remove (or ablate) the brain regions that give rise to seizures. Multiday invasive intracranial recordings using surgically implanted arrays of subdural or depth electrodes that capture the patient's typical seizures are typically necessary to localize the seizure onset zones (SOZs) in the brain and define surgical targets[3]. The limited spatial sampling of the brain that is possible using implanted electrode arrays and reliance on visual analysis of ECoG data in current clinical practice make SOZ determinations from seizure recordings only an approximation of the seizure-initiating networks. In turn, seizure-initiating networks themselves are only a surrogate for the hypothetical epileptogenic zone (EZ), the minimal amount of tissue that must be resected to produce seizure freedom[3,4]. In some cases, complete surgical resection of the SOZ may be prevented by the proximity of functionally important brain tissue. However, even when resections of the SOZ are deemed satisfactory, long-term seizure freedom after epilepsy surgery remains less than desirable, with seizure recurrence being common in a substantial proportion of patients, especially those with non-lesional epilepsy or SOZs that are outside the temporal lobes[5,6]. On the other hand, there are also instances where an incomplete resection of the presumed SOZ yields seizure freedom. These observations only further highlight the fact that SOZs represent only an approximation of the optimal tissue to resect or ablate. Seizure recurrence after epilepsy surgery is to a large extent attributable to residual pro-epileptic tissue that was

[1]Department of Neurology, Medical College of Wisconsin, Milwaukee, WI 53226, USA. [2]Department of Neurosurgery, Medical College of Wisconsin, Milwaukee, WI 53226, USA. [3]Department of Biomedical Engineering, Marquette University and Medical College of Wisconsin, Milwaukee, WI, USA. ✉email: mraghavan@mcw.edu

not identified by the pre-surgical evaluation process[6]. There are thus strong incentives to seek novel ways to map the full extent of epileptogenic networks in the brain in focal epilepsy[7–9].

We conceptualize the problem of mapping epileptogenic networks as one of mapping hyperexcitability across the brain[10]. By hyperexcitability, in this paper, we specifically mean increased responsivity of the cortex to afferent excitation that may be attributable either to increased cortical gain, or impaired gain-control mechanisms. Non-invasive methods for determining cortical excitability are predominantly limited to primary sensory or motor cortices, where responses to sensory or transcranial magnetic stimuli can provide regional measures of excitability[11,12]. In patients with focal epilepsy who undergo invasive intracranial EEG studies, the presence of cortical hyperexcitability has traditionally been inferred from surrogate markers of intrinsic excitability such as epileptic spike activity or seizure initiation[3]. Over the last couple of decades, bursts of high-frequency oscillations (HFOs) in the gamma and higher frequency bands have been recognized as another phenomenon that might point to intrinsic excitability, although physiological gamma band activity presents a confound that may undermine their specificity[13,14]. Induction of electrographic or clinical seizure phenomena by direct electrical stimulation of the brain is another clinical approach that has been explored for identifying cortical hyperexcitability but has major limitations[15,16]. Responses to single pulse electrical stimulation (SPES) of the cortex, and more recently, cortico-cortical evoked potentials (CCEPs) elicited by sequential electrical stimulation of different pairs of electrodes within intracranial electrode arrays have also shown promise as a method to map hyperexcitable networks in focal epilepsy[17–20]. In contrast to these approaches, many studies have sought to characterize epileptic networks in the brain using functional connectivity (FC) analysis applied to intracranial recordings. The large body of evidence for network alterations in epilepsy due to cortical hyperexcitability[21,22] makes FC a particularly promising approach for revealing novel insights into epileptogenic networks. However, FC based on physiological signals such as EEG, MEG, or ECoG has been defined using many different methods[23,24]. These methods make different assumptions about the nature of neural interactions across the brain, have differing vulnerabilities to volume-conducted signals and noise, and yield connectivity estimates that may be either directed or undirected[25]. Based on FC defined by any of these methods, several graph-theoretic metrics may be estimated to gain insights into the underlying networks[26]. Several recent studies have examined the relationship between seizure-initiating brain regions and graph metrics derived from different ECoG connectivity measures with encouraging results[27–34]. Differences in the choice of connectivity measures and the lack of clear predictions to motivate these choices make it challenging to draw generalizable conclusions about the relationship between measures derived from FC and cortical hyperexcitability.

Although many measures of FC have been defined based on different signal processing considerations, the inferences about FC in the brain that any method yields are reliable only to the extent that assumptions implicit in the method are true for the brain. It is well known that although ECoG, EEG, and MEG signals arise from the spatiotemporal summation of excitatory and inhibitory post-synaptic potentials in the cortex, not all components of these signals are directly related to local neuronal firing rates. There is compelling evidence, however, that ECoG and local field potential (LFP) power in the gamma frequency band (40–200 Hz) is indeed correlated to the firing rates of local neuronal populations[35–39]. We hypothesize that in the interictal state, hyperexcitability increases temporal correlations in the firing rates of neuronal populations within the EZ due to mutual excitation. The notion of increased neuronal synchrony within the epileptic cortex has been around for decades but has typically been invoked as a mechanism underlying the generation of epileptic spikes or transitions to the ictal state[40,41]. If hyperexcitability increases firing-rate correlations under all conditions within the EZ, we should expect to see higher correlations of gamma power between ECoG signals recorded from within the SOZ compared to those from relatively normal cortical regions. Any such increase should be discernable using amplitude envelope correlations (AECs), a relatively simple measure of functional connectivity. We tested this prediction using interictal samples of ECoG from a cohort of patients with drug-resistant epilepsy who experienced excellent seizure outcomes following removal of the brain regions that were identified as seizure onset zones (SOZs). For each patient, we estimated FC in eight frequency bands spanning 4–290 Hz using narrow-band amplitude envelope correlations (AECs). From these FC matrices, we estimated four graph metrics each and then studied the relationship between SOZs and connectivity estimates as well as the derived graph metrics. We contrasted our findings based on AECs to those derived from phase-locking values (PLVs), a measure of phase coupling of narrow-band ECoG activity across brain locations. We selected PLVs for this comparison since it is representative of a class of connectivity measures that depend purely on the narrow-band phase of the ECoG signals with no dependence on the amplitude of the signal envelopes.

Methods

Patients

Our patient cohort consisted of 26 adults above the age of 18 years with drug-resistant focal epilepsy who underwent invasive EEG recordings before resective epilepsy surgery at the Comprehensive Epilepsy program of the Medical College of Wisconsin, Milwaukee, WI, USA. This study was performed under a study protocol approved by the Institutional Review Board of the Medical College of Wisconsin (PRO15813) and all research activities were conducted in compliance with relevant guidelines and regulations. Informed consent was obtained from all patients and/or their legal guardians. Patients were selected after applying a set of inclusion and exclusion criteria to all those who underwent invasive EEG recordings for refractory epilepsy over a period of 10 years between 2008 and 2018. Since our epilepsy surgery program switched from almost exclusively subdural invasive EEG recordings to stereo-EEG studies with depth electrodes during the latter portion of this 10 year window, we included only invasive studies performed primarily using subdural grid recordings for this study. Three patients, however, did have additional depth electrodes sampling the mesial temporal regions, and data from these electrodes were included in our analysis. Only patients who maintained Engel Class IA seizure outcomes

for ≥ 2 years were included. A further key inclusion criterion was the availability of an awake sample of ECoG data from within the first 24 h of the recording that was at least 2 h removed from any recorded seizures. Perioperative ischemic strokes at the resection margins and epilepsy secondary to high-grade tumors were exclusion criteria. Twenty-six patients who fulfilled these criteria were included in the study. The characteristics of our patient cohort are summarized in Table 1. Demographic and epilepsy variables for individual patients are provided in Table S1 (see Supplementary material online).

Invasive-EEG recordings

All patients underwent multi-day invasive Video-EEG recordings using Nihon Kohden *Neurofax* EEG acquisition systems (Nihon Kohden, Tokyo, Japan) with 128 or 192 channel amplifiers, and surgically implanted subdural grid and strip electrodes. The subdural electrodes were platinum-iridium alloy electrode discs (4 mm diameter) arranged in a grid (8 × 8), partial grid (8 × 2), strip (4 × 1 or 6 × 1), or a combination of both types of electrodes (Ad-Tech Medical, Racine, Wisconsin, USA). In some patients, contacts at the corners of grids, or entire grid rows were removed during the implantation depending on the desired coverage at the discretion of the neurosurgeon. Three patients had additional depth electrodes sampling the mesial temporal structures. A 2-channel electrode that was anchored to the bone at the craniotomy margin with titanium screws served as a system reference. All EEG recordings were performed at a sampling rate of 1000 Hz. EKG and video data were simultaneously acquired. The patients were observed in a Neurological Intensive Care Unit during these studies and anticonvulsants were tapered to varying degrees to provoke habitual seizures to localize the seizure onset zones. After adequate seizure data was captured, patients were placed back on their anticonvulsant regimens and returned to the operating room for ablative procedures after completing bedside electrical stimulation mapping of functional cortices when clinically necessary. The archived data from these studies typically included daily 30 min awake and asleep interictal ECoG samples, in addition to the segments containing clinical events or electrographic seizures and the recordings during electrical stimulation mapping of the cortex. This study utilized the awake 30 min samples from within the first 24 h of the recording that were available for all patients in our cohort.

Electrode localization

All patients underwent a high-resolution CT and MRI of the brain after the implantation of intracranial electrodes. The locations of the implanted electrodes were reconstructed for all patients at the time of their invasive EEG studies using CT-MR co-registration methods that have been described elsewhere[42]. Our method uses high-resolution CT and MR imaging data acquired after implantation of the subdural electrodes. MRI volumes are first segmented using Freesurfer (https://surfer.nmr.mgh.harvard.edu/). CT data are co-registered to the MRI volume using the mutual information algorithm in FLIRT (https://fsl.fmrib.ox.ac.uk/fsl/fslwiki/FLIRT) before a threshold is applied and the data binarized to retain just the subdural electrodes. The MRI and electrode masks derived from CT are displayed in 3DSlicer (http://www.slicer.org). The CT-MR co-registration data for visualizing

Patient characteristics	
Mean age (years)	35.5 (+/− 12.1)
Gender	
Female	46%
Male	54%
Age at seizure onset (years)	16.7 (+/− 10.1)
MR Imaging lesions	
Non-lesional	9 (34.6%)
Cortical malformations	5 (19.2%)
Mesial temporal sclerosis	4 (15.4%)
Low-grade tumors	3 (11.5%)
Vascular malformations	3 (11.5%)
Encephalomalacia	2 (7.7%)
SOZ laterality (hemisphere)	
Left	14 (53%)
Right	12 (47%)
SOZ locations (lobe)	
Temporal lobe	19 (73%)
Temporal plus	4 (15%)
Extratemporal	3 (12%)
Age at surgery (years)	35.5 (+/− 12.1)
Post-op follow-up (years)	7.5 (+/− 3.1)

Table 1. Summary characteristics of the patient cohort. Standard deviations of the duration variables are provided in parentheses. Demographic and epilepsy variables at the level of individual patients are provided in the Supplementary material online as Table S1.

electrode locations as well as post-operative MR imaging data for all patients were retrieved and reviewed by an epileptologist to determine the position of electrodes relative to the resected brain volumes.

Clinical variables and ECoG samples

Clinical epilepsy variables for all patients were retrieved from the electronic medical records and are provided in Table S1 (see Supplementary material online). For this study, the clinical reports and schematic maps generated during the invasive EEG studies were reviewed by an epileptologist. Brain imaging data relevant to the location of implanted electrodes and post-operative resection volumes were also reviewed for each patient. ECoG data analyzed in this study were the first 30 min sample of awake recording from within the first 24 h of the invasive EEG recording. Before being exported, the ECoG data were first reviewed visually by an experienced electroencephalographer using the Nihon Kohden review software on a referential montage, and noisy channels were eliminated. The data was then exported as ASCII text files and transferred to a workstation for further analysis using custom scripts written in MATLAB (The MathWorks, Inc., Natick, Massachusetts, United States).

SOZ and RZ maps

Our SOZ definitions for each patient are based on the electrodes that were determined to be part of the SOZ at the time of the surgical evaluation. At our epilepsy center, clinical SOZ determinations are based on the consensus opinion of two or more epileptologists who have reviewed the seizure recordings. No secondary analysis of ictal recordings was performed for this study. The SOZ map for each patient was a binary mask over the electrode label list, with 1 designating a channel that was deemed to be in the SOZ. For each patient, based on a careful visual review of the intracranial electrode visualizations from CT-MR co-registration and post-operative MR imaging by an epileptologist on the study team, electrodes that were within the eventual resection zone (RZ) were identified and a binary mask was created for the RZs. Given the frequent presence of gliosis at surgical resection margins, electrodes that were within 0.5 cm of the resection margins were assigned to the RZ.

Functional connectivity estimation

ECoG data from each patient was analyzed using custom scripts written in MATLAB (Mathworks, Natick, MA, USA) that were supplemented by functions from *EEGLAB* (https://sccn.ucsd.edu/eeglab/) and *FieldTrip* (http://www.fieldtriptoolbox.org/). The exported ECoG data from each patient was first loaded into a MATLAB data structure along with corresponding binary masks defining the SOZ and RZ contacts. The ECoG data was visually inspected by an epileptologist using display routines from *EEGLAB*, and channels containing continuous artifacts, or excessive line noise were excluded. A line-noise filter was then applied to the data to remove the first 5 harmonics of power line artifacts using the spectrum estimation method described by Mewett et. al.[43] as implemented in the *removeLineNoise_SpectrumEstimation* MATLAB function which is publicly available (https://www.mathworks.com/matlabcentral/fileexchange/54228-remove-line-noise). We chose a spectrum estimation method for line noise removal since it is less prone to produce distortions of the time domain signal compared to traditional notch filters. After line-noise filtering, the ECoG data was re-referenced to a common average reference. The continuous ECoG samples were screened for epochs (of 12s duration each) containing high amplitude transients (> 3000 microvolts), which were tagged for later exclusion from calculations of FC. We did not explicitly detect and tag epochs containing epileptic spikes or pathological high-frequency oscillations (HFOs) for exclusion from our analysis. All analysis was carried out at the original signal sampling rate of 1000 Hz. To calculate FC for the ECoG samples from each patient, the data was first bandpass filtered to each of 8 frequency bands: 4–8 Hz, theta; 8–12 Hz, alpha; 15–25 Hz, beta; 35–50 Hz, low-gamma;70–110, high-gamma 1; 130–170 Hz, high-gamma 2; 190–230 Hz, high gamma 3; and, 250–290 Hz, fast-ripple band. We divided the gamma band into three separate sub-bands for our analysis for computational reasons. Given the 1/frequency drop-off in ECoG spectral power, without some kind of spectral equalization, amplitude envelope estimates from broadband signals will disproportionately represent the lower frequencies. Furthermore, amplitude envelope estimates using the Hilbert transform degrades with increasing bandwidth. Finally, we wished to avoid frequencies where the signal could potentially have been impacted by harmonics. The narrow band definitions that we use allow us to minimize these concerns. Filtering was done using the *FieldTrip* function *ft_preproc_bandpassfilter* set to perform two-pass (zero phase-shift) FIR filtering, with the filter order set to five. For each frequency band, the narrow-band ECoG data was then divided into 12s nonoverlapping epochs, and previously tagged noisy epochs were excluded. The two FC metrics employed in this study are both derived from the Hilbert transform of the band-passed ECoG signals. To minimize edge effects the ECoG data epochs were mirror-padded at both ends before being Hilbert transformed. The mirror-padding was then trimmed to retrieve the Hilbert-transformed 12s epochs. The amplitude envelopes and instantaneous phase of the ECoG signals were determined from the Hilbert transforms of the signals. The cross-channel Pearson correlation of the amplitude envelopes was calculated and averaged across epochs to estimate the Amplitude Envelope Correlations (AECs). Phase-locking values were calculated using the definition for resting state PLV[44–47] and likewise averaged across epochs. For a band-limited pair of signals, $x(t,f)$ and $y(t,f)$, whose Hilbert transforms are $H[x(t,\ f)]$ and $H[y(t,f)]$ respectively, the AEC value is defined as follows:

$$AEC\big(x(t,\ f),y(t,\ f)\big) = \big\langle corr\big(\big|H[x(t,\ f)]\big|,\ \big|H[y(t,\ f)]\big|\big)\big\rangle \tag{1}$$

The corresponding PLV value for the two band-limited signals is defined as follows:

$$PLV(x(t,f),y(t,f)) = \left\langle \frac{1}{T}\left|\sum e^{i(\phi_x(t,f)-\phi_y(t,f))}\right|\right\rangle \tag{2}$$

Here, $\phi_x(t,f)$ and $\phi_y(t,f)$ are the instantaneous phases of the two band-limited signals derived from their analytic signals. The results of our estimation of PLV were virtually identical to those produced by the publicly available fast FC toolbox, *fastFC*[48]. The connectivity matrices that both these FC measures yield for each patient are weighted and undirected. A preliminary analysis of the stability of the connectivity matrices found that the correlation between matrices estimated from a sub-sample of epochs and those based on all available epochs reached > 99% by ~ 100 epochs(~ 20 min of data). Our ECoG analysis pipeline is depicted in Fig. 1. After the exclusion of noisy channels, there were a total of 2176 channels of ECoG data available for analysis over our patient cohort. Of these, 344 were SOZ channels.

AEC and PLV connectivity weights

For each frequency band, we compared the mean values of the connection weights between nodes within the SOZ, between nodes outside the SOZ, and for connections linking these two subnetworks. The calculations were performed at the level of individual patients and then averaged across patients. The statistical significance of the difference was assessed using a paired sample Wilcoxon test at an alpha of 0.05 that was adjusted for multiple comparisons. We also estimated the ratio of the mean FC weights (mean FC weight within SOZ nodes/mean FC weights outside SOZ). To reject the possibility that the higher mean AEC values within the SOZ network could potentially arise trivially because SOZ node pairs tend to be closer to each other on the aggregate compared to non-SOZ node pairs (and therefore potentially more correlated), we performed an analysis of adjacent-channel AEC values for the SOZ and non-SOZ networks. The non-SOZ network in this case excluded the nodes within the resection zones (RZ). We generated pairs of bootstrap distributions (SOZ vs non-SOZ) for the mean value of adjacent-node AEC values across patients. For the SOZ distribution, samples of the bootstrap distribution were generated by resampling of the 26 intra-subject means of adjacent-node AEC values for the SOZ networks 10,000 times. A bootstrap distribution was similarly generated for the non-SOZ network. The separation between the pairs of bootstrap distributions was characterized using a discriminability index d' defined for the case of unequal variances. The d' value is defined by the following equation:

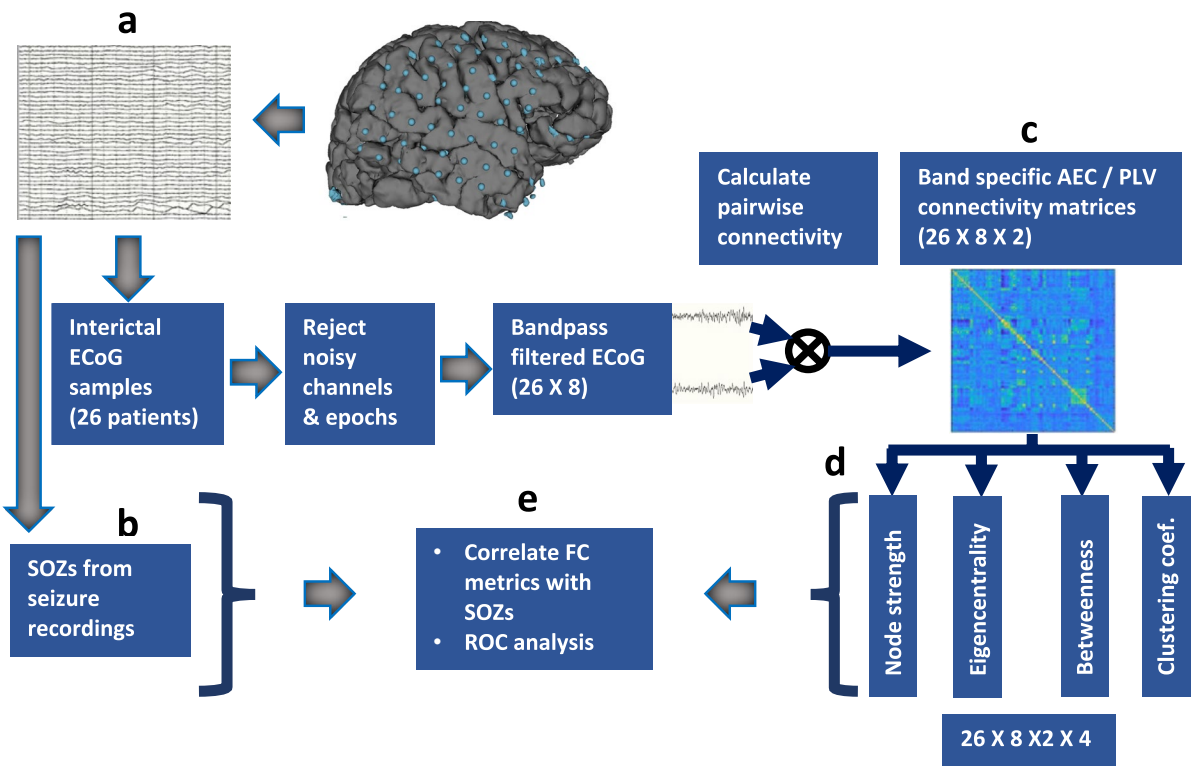

Figure 1. ECoG analysis pipeline. (**a**) ECoG data from each patient consisted of 30 min samples acquired in the awake state within the first 24 h of the invasive EEG recording. (**b**) For each patient, the designation of seizure onset zone (SOZ) channels of the ECoG data was based on those established by the clinical epilepsy team at the time of the patient's surgery. No reanalysis or secondary review was performed for this study. After eliminating noisy channels and tagging noisy epochs, ECoG signals were re-referenced to a common average reference. The signals were bandpass filtered to each of eight frequency bands spanning 4.0 to 290 Hz and divided into 12s epochs. Epochs tagged as being excessively noisy were eliminated at this stage. Instantaneous values of signal amplitude envelopes and phase were estimated from the Hilbert transforms of the signals. (**c**) For each frequency band, connectivity matrices based on Amplitude-Envelope Correlations (AECs) and Phase-Locking Values (PLVs) were calculated and averaged over epochs. (**d**) Four graph metrics, node-strength, eigencentrality, betweenness centrality, and clustering coefficient were estimated from the connectivity matrices for each frequency band. (**e**) The values of AECs, PLVs, and the derived graph metrics for the SOZ and non-SOZ subnetworks were compared using permutation testing and ROC analysis.

$$d' = |\mu_1 - \mu_2| \Big/ \sqrt{(\sigma_1^2 + \sigma_2^2)/2} \tag{3}$$

Here μ_1 and μ_2 are the means of the two bootstrap distributions while σ_1^2 and σ_2^2 represent the corresponding variances.

Graph metrics

For each patient, frequency band, and measure of connectivity we calculated four graph-theoretic metrics from the FC matrices using the Brain Connectivity Toolbox[49]. The metrics estimated were node strength, eigenvector centrality (eigencentrality), betweenness centrality, and clustering coefficient. For undirected connectivity measures, node strength is simply the sum of all the connection weights to (or from) any given node. It provides a measure of how strongly a node is connected to other nodes within the network. The eigenvector centrality (or eigencentrality) of a node is a measure of its influence on the network. A node with a high eigencentrality score is connected to many nodes that themselves have high eigencentrality. The betweenness centrality of a node is a measure of how many shortest paths between other nodes include this node: nodes with high betweenness centrality have a greater influence on the interactions between other nodes. The local clustering coefficient of a node provides a measure of how closely connected the network around a given node is. No threshold was applied to the FC matrices before estimating these graph metrics. Node strength values for each patient were normalized by the number of channels to account for differences in ECoG channel count across patients. For the calculation of betweenness centrality, the inverse of the connectivity matrix was used as the input since higher correlation connections are interpreted as shorter distances.

Analysis of graph metrics

We compared the mean values of the estimated graph metrics at the channels designated as SOZ to those outside the SOZ for the eight different frequency bands by first calculating the contrast of the difference between the mean values of the metric for the SOZ and non-SOZ ($\sim SOZ$) nodes (channels. For frequency-band fb, connectivity measure cm, and graph metric gm, the value of the contrast of the graph metric is defined as follows:

$$C(fb, cm, gm) = \left[\frac{\langle G_{SOZ}(fb, cm, gm) \rangle - \langle G_{\sim SOZ}(fb, cm, gm) \rangle}{\langle G_{SOZ}(fb, cm, gm) \rangle + \langle G_{\sim SOZ}(fb, cm, gm) \rangle} \right] \tag{1}$$

Here $\langle G_{SOZ}(fb, cm, gm) \rangle$ is the mean value of the graph metric for the SOZ nodes (channels), and $\langle G_{\sim SOZ}(fb, cm, gm) \rangle$ is the corresponding mean value for the non-SOZ nodes. All of the graph metrics have strictly positive values. As such, the values of the contrast are constrained between -1 and $+1$. The contrasts were calculated for individual patients and then averaged across the group. For each connectivity measure and frequency band, we generated permutation test null distributions of the average contrast metric across patients by randomly shuffling the designation of SOZs within each patient and re-estimating the mean contrast value for the group 10,000 times. The observed value of the mean contrast for the true SOZ nodes was then used to estimate Z-score deviations relative to the permutation test null distributions. To gain insight into the individual variation of these graph metrics across patients we also plotted the mean values of the measures in the SOZ and outside the SOZ along with the median values and quartile ranges.

ROC analysis

Finally, we performed ROC analyses to determine the sensitivity and specificity of the estimated graph metrics for identifying SOZ nodes. ROC analyses were performed for individual patients to estimate the area under the ROC curve (AUCs) before averaging these values across patients. The mean and standard deviations of the AUCs based on the four different graph metrics were estimated for the different frequency bands. We estimated the p values of the AUCs by comparing the observed means of the AUCs against a permutation test null distribution that was generated by repeated estimations of the mean AUCs after randomizing the SOZ designations in each patient 5000 times. No transformations were applied to the graph metrics for ROC analyses performed at the level of individual patients. We, however, also performed a secondary analysis where the ROC curves were based on data that was pooled across all patients. Since the absolute values of the graph metrics can potentially vary systematically across patients, we rescaled the values of the metrics in individual patients to a (0,1) range before pooling the data from all patients. An approach for making graph measures comparable across subjects based on Minimum Spanning Trees of the FC matrices has been proposed by some authors[50]. We therefore recalculated AEC-based node strengths across the gamma band after first generating Minimum Spanning Trees using inverted FC weights, and then using the original values of the retained connections to estimate the graph metrics which were then normalized by their maximum values. ROC analysis for detection of the SOZ was repeated using the node strengths generated using the MST approach. The resulting AUC values were compared to those observed from our ROC analysis using pooled data with within-subject (0,1) rescaling of the graph metrics.

Results

Patient cohort

Our patient cohort consisted of 14 male (54%) and 12 female (46%) patients. The mean age at seizure onset was 16.7 years (± 10.1 years) and the mean age at the time of surgery was 35.5 years (± 12.1 years). The mean duration of follow-up was 7.5 years (± 3.1 years). Structural abnormalities were evident on magnetic resonance imaging in 17/26 (66%) patients (malformations of cortical development in 5; mesial temporal sclerosis in 4; low-grade

gliomas 3; vascular malformation 3; encephalomalacia 2). Laterality of the SOZ and resections was on the left in 14 patients (53%). The location of SOZs and the subsequent surgical resections were in the temporal lobe in 19/26 (73%) patients, temporal-plus in 4 (15%), and extratemporal in 3 (12%). All patients had remained seizure-free (Engel Class IA) outcomes for at least 2 years after their surgeries. Summary characteristics of our patient cohort are provided in Table 1. Demographic and clinic variables for individual patients are provided in Table S1 (see Supplementary material online).

AEC and PLV values within and outside the SOZ

The mean values of AECs (averaged across patients) and PLVs within the SOZ (SOZ subnetwork) and outside the SOZ (non-SOZ subnetwork) are plotted across different frequency bands in Fig. 2a and b. Also plotted are the mean values of the AECs and PLVs for connections between the two subnetworks. Both AEC and PLV values are significantly higher within the SOZ subnetwork compared to the non-SOZ subnetwork across all frequency bands. Using a paired sample Wilcoxon tests (one-tailed) with an alpha of 0.05 that was adjusted for multiple comparisons the values of AECs within the SOZ were significantly higher for all frequency bands (p-values ranged from 0.0008 for the 4–8 Hz band, to 0.000004 for the 30–50 Hz band). The values of PLVs were also significantly higher within the SOZ compared to areas outside the SOZ for all frequency bands (p value ranged from 0.004 for the 250–290 Hz band to 0.0001 for the 15–25 Hz band). Between-network mean AEC values (connections between SOZ and non-SOZ nodes) are nearly identical to those for the non-SOZ subnetwork

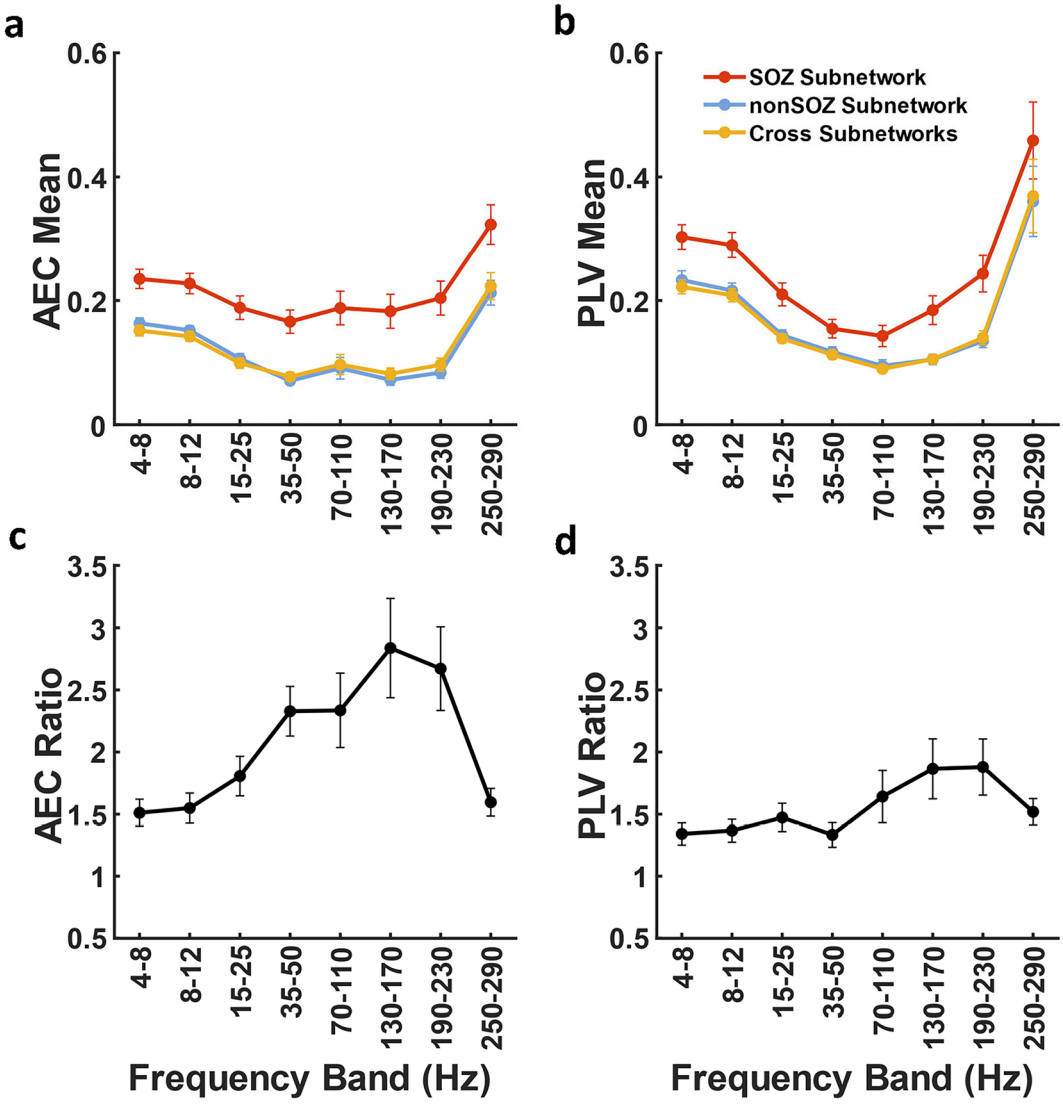

Figure 2. AECs show stronger increases between SOZ nodes compared to PLVs. (**a**) Mean values of AECs for connections between SOZ nodes, between non-SOZ nodes, and across these two classes of nodes for different frequency bands. (**b**) The corresponding plots for PLVs. (**c**) The ratios of mean AECs inside and outside the SOZ. (**d**) The ratios of mean PLVs inside and outside the SOZ. The error bars in these plots represent the standard error.

indicating that while nodes within the SOZ network are strongly connected, their connections to nodes outside the SOZ are not significantly increased in strength.

The ratios of the AECs and PLVs (between the SOZ and non-SOZ) networks are plotted in Fig. 2c and d across frequencies. Mean AEC values both within and outside the SOZ drop substantially in the gamma frequency bands, but the magnitude of the difference between them remains approximately the same. This translates into a much higher ratio of mean SOZ AEC values relative to mean non-SOZ connections across the gamma band as seen in Fig. 2c. The peak value of the ratio is in the high gamma band (130–170 Hz). A similar effect, but of a smaller magnitude, is seen for mean values of PLVs within and SOZ and outside the SOZ as shown in Fig. 2b and d.

Adjacent channel AEC values within and outside the SOZ

One possible explanation for the strongly elevated AEC values within the SOZ subnetwork is that gamma-band AECs may simply be higher between nodes that are physically close to each other compared to distant pairs of nodes. If this is the case, higher mean values of AECs within the SOZ network of nodes could arise trivially because they are spatially closer together compared to node pairs outside the SOZ on the aggregate. To exclude this possibility, we examined bootstrap distributions for the mean AEC values within and outside the SOZ exclusively for adjacent pairs of nodes (so the inter-electrode separation is the same across all node pairs). The pairs of SOZ and non-SOZ bootstrap distributions show a robust separation of their means across the gamma band (d' values ranging from 4.08 for the 35–50 Hz band to 4.48 for the 190–230 Hz band) as shown in Fig. 3a and b. The pooled distributions of the log-transformed adjacent-node AEC values for the SOZ and non-SOZ networks are shown in Fig. S1 (see Supplementary material online).

Contrast of graph metrics within and outside the SOZ

Across all ECoG channels, the contrast of the graph metrics between SOZ and non-SOZ nodes derived from AECs show a markedly stronger frequency dependence relative to those derived from PLVs. Figure 4a and b show the contrast values for the graph metrics derived from AECs and PLVs respectively, plotted across the eight frequency bands. The corresponding Z-scores relative to permutation test null distributions are shown in Fig. 4c and d. Node-strength, eigencentrality, and clustering coefficient derived from AECs show a sharp and significant rise starting in the low-gamma band (35–50 Hz) (Z-score > 8.0 relative to the permutation null distribution) and remains elevated throughout the gamma frequency bands (Z-score > 6.0) with slight a drop seen above 230 Hz. Interestingly, although the peak ratio of AEC values within the SOZ network relative to those between non-SOZ nodes is maximal in the high gamma band (Fig. 2), the peak Z-scores of the contrast value for three of the four graph metrics occur in the low-gamma band (Fig. 4c; permutation test Z-scores > 8.0). This derives from the lower variance of the graph measures in the low-gamma band. Betweenness centrality derived from AECs also shows marked increases within the SOZ in the gamma frequency band, but corresponding Z-scores relative to permutation test distributions only reach modest significance in the gamma band. For PLV-based graph metrics, the increases of node strength, eigencentrality, and clustering coefficients are significant only in the high gamma band, but the magnitude of the effect is much smaller (maximal contrast Z-scores ~ 4.0) than for the corresponding AEC-based metrics. PLV-based betweenness centrality shows a more complex profile across frequency, with a minimum in the alpha band (8–12 Hz) and slight elevations noted from 35 to 200 Hz but neither of these changes are statistically significant at $p < 0.01$.

The mean values of the graph metrics derived from AECs for the SOZ and non-SOZ nodes are plotted as box and whisker plots in Fig. 5. In these plots, the open and filled circles indicate values inside and outside the SOZ respectively, with gray lines linking the data-points for individual patients. We note that there is far greater variance of all graph metrics at the SOZ nodes relative to non-SOZ nodes. Despite the robust elevations of SOZ versus non-SOZ average contrast values for three of the graph metrics across all patients (shown in Fig. 4c), there are patients in our cohort for whom the mean values are either not elevated or are lower within the SOZ nodes in the low gamma band. These instances were not predicted by the duration of epilepsy, location of the seizure onset zones, or lesion type.

Discriminability of the SOZs

We performed receiver operating characteristic (ROC) analyses in individual patients to assess the discriminability of the SOZ nodes in different frequency bands based on the graph metrics calculated from untransformed connectivity matrices. and then averaged the AUCs. The mean AUC values for the different graph metrics derived from AECs and PLVs are shown plotted in Fig. 6a and b respectively for the different frequency bands. As might be expected from Fig. 4c, the peak AUC values for discriminating the SOZ nodes using AEC-based graph metrics occur in the low-gamma (35–50 Hz) band. In this frequency band, we find mean AUCs (across all patients) between 0.71 and 0.73 for detecting the SOZ using node strength, eigencentrality, and clustering coefficient. These graph metrics are also strongly correlated to each other (r > 0.9). By contrast, PLV-based graph metrics showed weaker discrimination of the SOZ channels and less pronounced frequency dependence. The average AUC values (across all patients) for node strength, eigencentrality, and clustering coefficient based on PLVs all peak ~ 0.62 across the gamma frequency band. The observed mean AUC values at different frequencies were compared to permutation test null distributions for this quantity (see Fig. S5 and Table S2 provided with the Supplementary material online). For the low-gamma (35–50 Hz) band Z-scores of the mean AUCs relative to the null distributions exceed 10.0 for node-strength, eigencentrality, and clustering based on the AECs. The Z-scores relative to the null distributions for AUCs for PLV-based graph metrics rise above 6.0 for the 130–170 Hz and higher band.

We also performed a secondary ROC analysis for graph metrics derived from AECs alone after rescaling the metrics from each patient to a (0,1) range to mitigate the impact of systematic differences in the absolute value

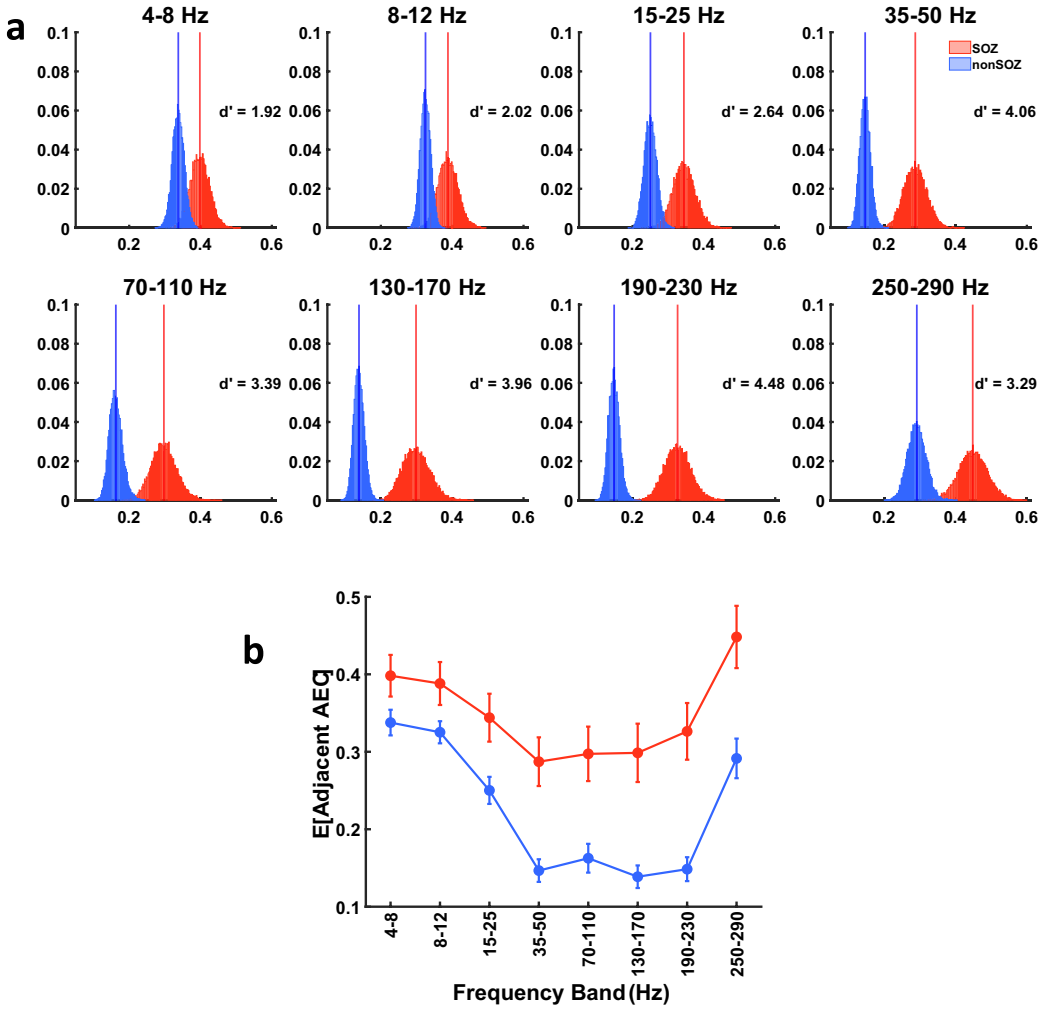

Figure 3. Across the gamma frequency range, adjacent-node AECs are significantly higher between the SOZ nodes compared to the non-SOZ nodes. (**a**) Pairs of bootstrap distributions for adjacent-node AECs for the SOZ and non-SOZ subnetworks. For each subnetwork, these distributions were generated by resampling the 26 intra-subject means of adjacent-node AEC values for the SOZ and non-SOZ networks 10,000 times. The discriminability index d' for each pair of distributions is shown on the plots. The d' value is defined by $d' = |\mu_1 - \mu_2| \Big/ \sqrt{(\sigma_1^2 + \sigma_2^2)/2}$. Here μ_1 and μ_2 are the means of the two bootstrap distributions while σ_1^2 and σ_2^2 represent the corresponding variances. (**b**) Means of the bootstrap distributions plotted as a function of frequency. The error bars indicate one standard deviation.

of graph metrics across patients and pooling the data from all patients. This analysis was performed only for the gamma band. The results are shown in Fig. 6c. For AEC-based node strength, a maximal AUC of 0.73 was seen in the 30–50 Hz frequency band. Since a Minimum Spanning Tree approach has been proposed for accomplishing the same objectives as the within-subject rescaling that we did by some authors[50], we recalculated AEC-based node strengths across the gamma band after generating within-subject Minimum Spanning Trees (MSTs) using inverted FC weights. After determining which connections to retain based on these MSTs, we used the retained un-inverted connection weights to estimate the graph metrics. The graph metrics were then normalized by the maximum values within the subject. ROC analysis applied to AEC-based graph metrics generated in this manner yielded lower values of AUCs in the range of 0.57–0.62 across the gamma band (maximal AUC of 0.62 in the 130–170 Hz band).

For AEC-based node strength, eigencentrality, and clustering coefficients in the low-gamma band we asked whether false positives from SOZ node detection using ROC analysis fall in the vicinity of the SOZ, as might be expected if there is a gradient of cortical hyperexcitability moving away from the SOZ. To answer this with the data at hand, we determined whether false positives at the optimal operating point on the ROC curves (defined as the intercept of the curve with the diagonal) fall disproportionately within the surgical resection (the RZ) compared to other locations. Pooling data across all subjects, there were 1832 electrodes outside the SOZ, of which 308 were within the RZ. Therefore, the likelihood of a SOZ-false positive being an RZ node (not including the SOZ nodes in the resection) by chance alone was 308/1832 (~ 16.8%). For the graph metrics that yielded the highest AUCs for discriminating the SOZs (NS, EVC, and CC) in the low gamma band, we determined the

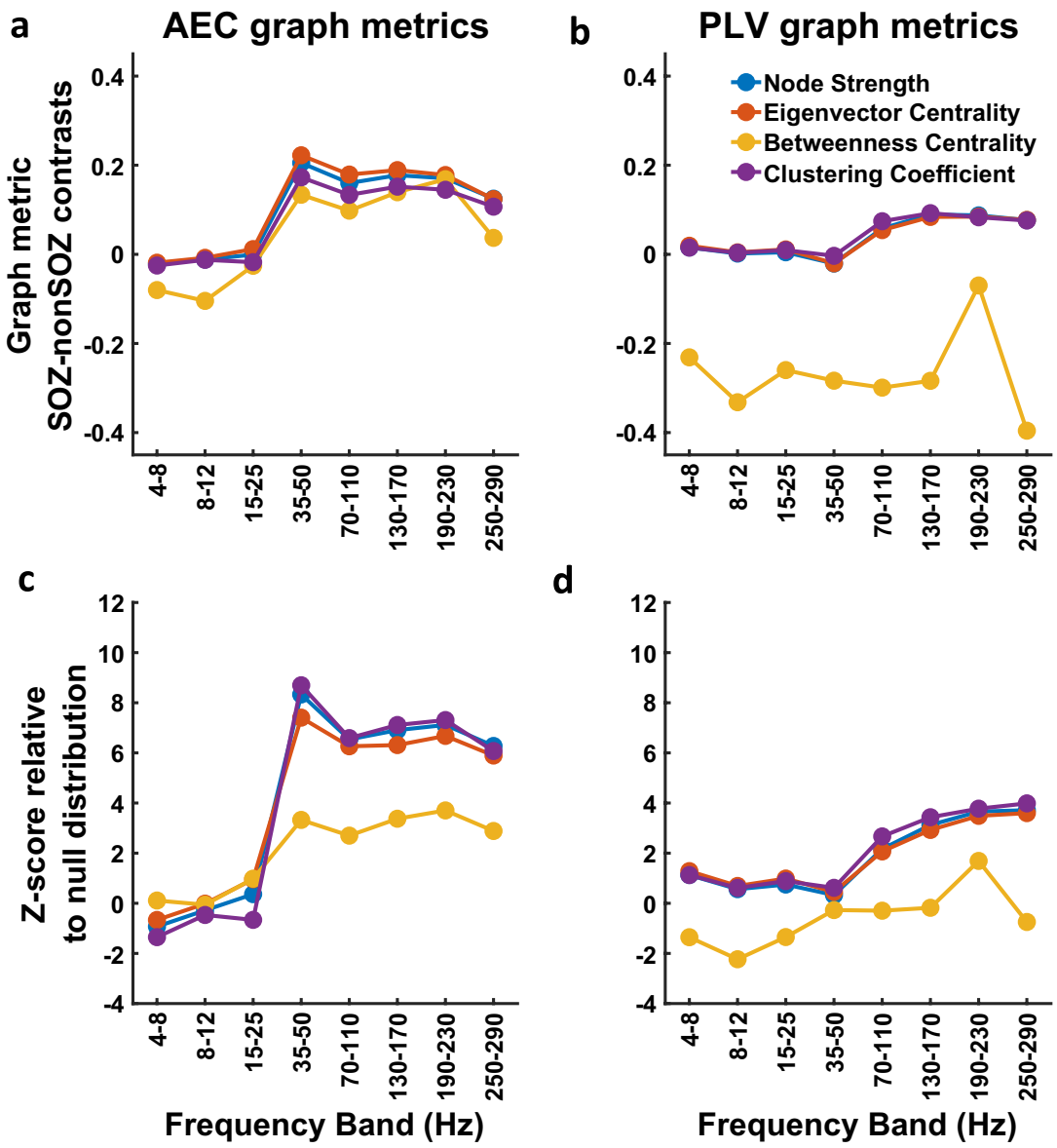

Figure 4. Contrast values of graph metrics derived from AECs and PLVs. (**a**) Graph-metric contrast values between SOZ and non-SOZ nodes for AECs using ECoG channels averaged across all patients, plotted across frequency bands. (**b**) Corresponding contrast values of PLV-based graph metrics. (**c**) Z-scores relative to permutation test null distributions for mean AEC-based graph-metric contrasts over all patients plotted across frequency bands. (**d**) Corresponding Z-scores of PLV-based graph metrics relative to permutation test distributions. For each connectivity measure and frequency band, we generated permutation test null distributions of the average contrast metric across patients by randomly shuffling the designation of SOZs within each patient and re-estimating the mean contrast value for the group 10,000 times. The observed value of the mean contrast for the true SOZ nodes was then used to estimate Z-score deviations relative to the permutation test null distributions.

percentage of SOZ false-positives at the ROC optimal operating point that were RZ nodes (excluding overlapping SOZ nodes). We then generated a permutation test null distribution for the percentage that would be expected to fall within the RZ by chance alone to estimate the Z-score deviations of the observed percentages relative to the null hypothesis. The observed values were 25.98% ($Z = 7.46$; $p = 8.26E-14$), 23.83% ($Z = 5.69$; $p = 1.24E-08$), and 26.58% ($Z = 7.69$; $p = 1.43E-14$) respectively for node-strength, eigencentrality, and clustering coefficients (see Fig. S4 provided with the Supplementary material online). This indicates that SOZ false positives from the ROC analysis of the graph metrics do indeed fall disproportionately in the RZ near the SOZ.

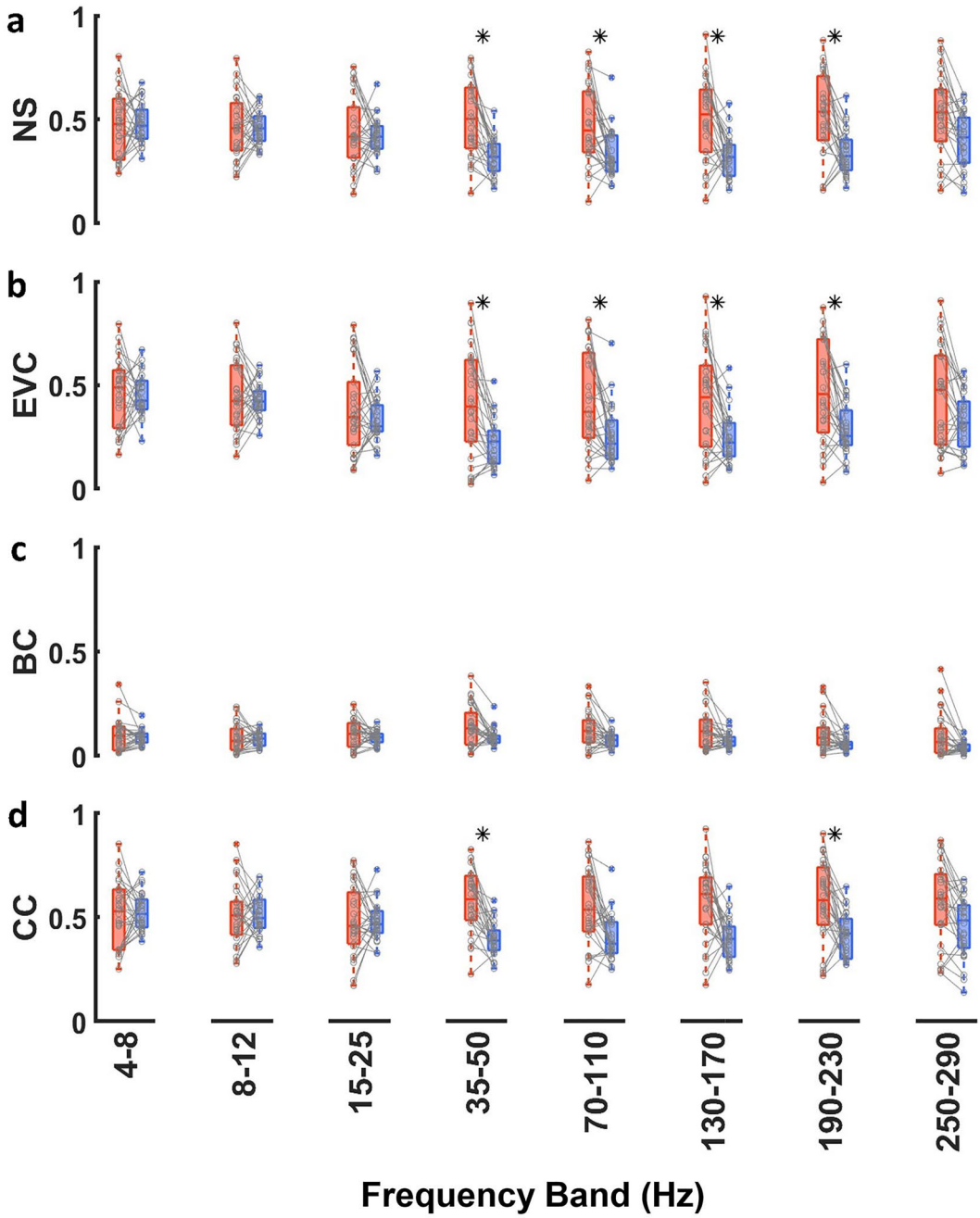

Figure 5. Comparison of AEC-based graph metric values for SOZ and non-SOZ channels for different frequency bands and graph metrics. (**a**) node strength, (**b**) eigenvector centrality, (**c**) betweenness centrality, (**d**) clustering coefficient. The box and whisker plots show the aggregate values for SOZ (red) vs non-SOZ (blue) channels. Grey markers and lines show individual patient comparisons. Asterisks denote significant differences between SOZ and non-SOZ channels ($p < 0.01$) using a paired sample Wilcoxon test with an alpha adjusted for multiple comparisons.

Discussion

Although ECoG signals are predominantly generated by spatiotemporal summation of post-synaptic membrane potential in the cerebral cortex, it is only in the gamma frequency bands that ECoG power shows strong correlations to the firing rates of local neuronal populations[35–39]. Gamma amplitude envelope correlations (AECs) thus provide an indirect measure of the firing rate correlations between neuronal populations across cortical locations. We hypothesized that focal cortical hyperexcitability in epilepsy increases firing rate correlations between neuronal populations within the epileptogenic network. This should be reflected as increased correlations of power (or amplitude) envelope in the gamma frequency bands within the SOZ in focal epilepsy. Increases in gamma activity driven by afferent inputs to the cortex are typically accompanied by a broader field of power decrements in the alpha and beta bands that have traditionally been referred to as alpha and beta desynchrony[51–54]. Because

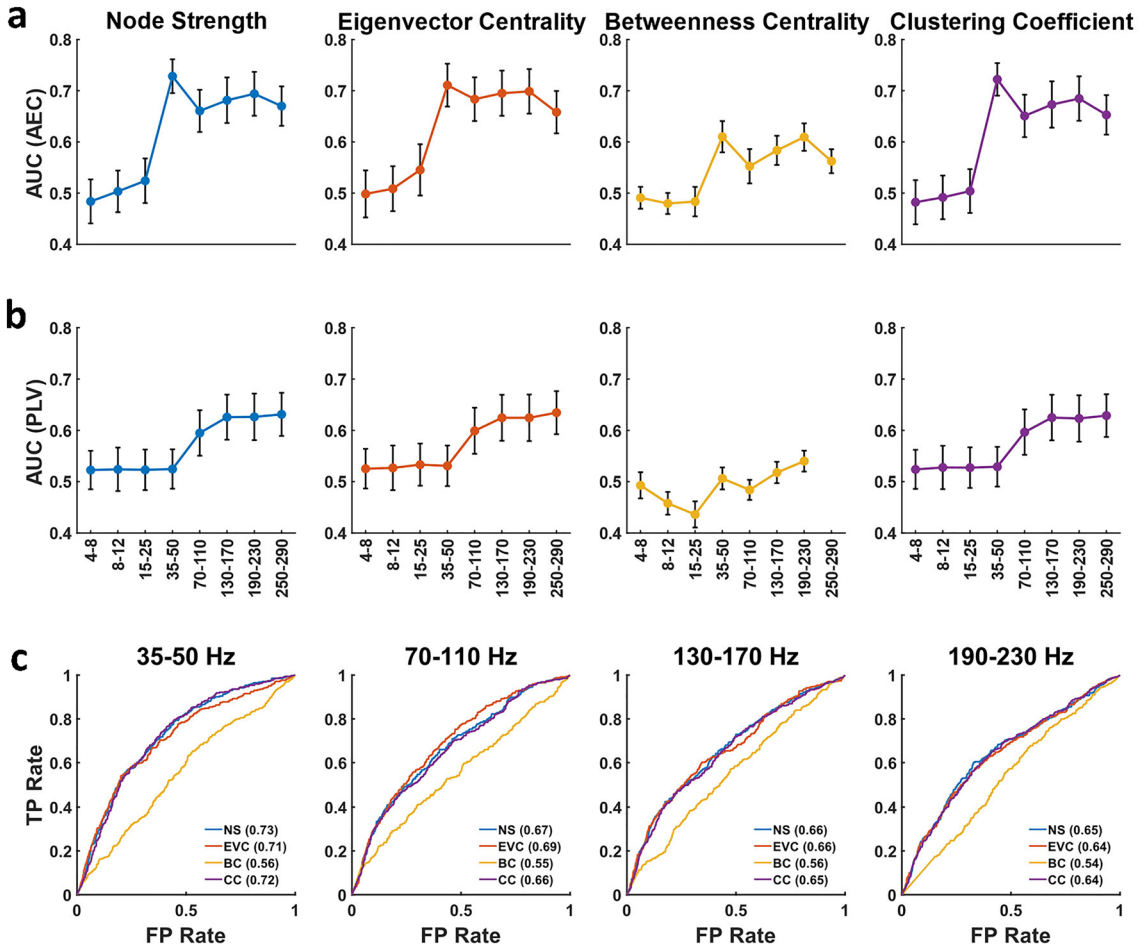

Figure 6. The area under the ROC curve (AUC) for SOZ node discrimination. Mean AUC values (across all patients) for graph metrics derived from (**a**) AECs and, (**b**) PLVs as a function of frequency. Peak values of the AUCs were observed in the low gamma (35–50 Hz) band for node strength (0.73), eigenvector centrality (0.71), and clustering coefficient (0.72). (**c**) ROC curves for discriminating SOZ nodes from AEC-based graph metrics across the gamma band using graph metrics pooled across all patients after rescaling to a (0,1) range within subjects. AUC values for the individual graph metrics are shown in parentheses with the line labels.

these effects are usually less localized than power increases in the gamma band, one may expect AECs at alpha and beta frequencies to show less pronounced changes within the hyperexcitable network. The effect of cortical hyperexcitability on narrow-band phase-phase coupling across cortical regions is harder to predict. There is strong evidence that the phase of cortical rhythms ranging from delta to beta frequencies can modulate gamma power and local neuronal firing rates[55–60]. There is also abundant evidence indicating that delta and theta band activity is increased in the epileptogenic cortex[61–65], and some recent studies suggest that phase-amplitude coupling may indeed be elevated within epileptic networks[66–68]. Nevertheless, in the absence of an explicit model for the mechanism of phase-phase coupling across cortical regions, these observations offer no straightforward prediction for PLV-based FC in hyperexcitable cortex.

In this study, we limited our epilepsy patient cohort to those who underwent intracranial EEG studies and experienced excellent seizure outcomes following surgical resection. This was to ensure that designated SOZs based on seizure recordings may be regarded as good approximations of the seizure-generating brain regions. We find that AECs are increased within the SOZ across all frequency bands, but the maxima of the ratio of mean AECs within and outside the SOZ is seen in the gamma band. Qualitatively similar, but much weaker effects are seen for connectivity defined from narrow-band phase synchrony using PLVs. We considered the possibility that, since SOZ nodes tend to be clustered together, higher mean AECs may arise trivially within the SOZ if AECs are generally higher between node pairs are that closer to each other. We rejected this possibility by comparing adjacent-node AEC values within and outside the SOZ so that all node pairs had the same approximate spatial separation. Bootstrap distributions for the adjacent-node AECs within and outside the SOZ show a prominent separation of their means specifically across the gamma band (from 35 to ~ 230 Hz), with higher values between SOZ nodes.

Contrasts of AEC-based graph metrics between the SOZ and non-SOZ locations show statistically robust increases only within the gamma band. The maximal Z-score deviations of the contrast values for AEC-based node strength, eigencentrality, and clustering coefficient based on permutation testing occur in the low-gamma band (Z-score > 8). These graph metrics are strongly correlated to each other ($r > 0.9$) suggesting that they most

likely provide mutually redundant information about cortical hyperexcitability. Betweenness centrality derived from AECs is also increased for the SOZ nodes across the gamma frequency band but shows only a weak positive correlation to the other three metrics. Despite the known inverse relationship between alpha and beta band power and gamma-band power during functional engagement of the cortex, we do not find significant increases or decreases of alpha and beta band contrasts of AEC-based graph metrics within the SOZ. By comparison to AEC-based graph metrics, the contrast values for PLV-based graph metrics show much weaker elevations in the gamma band (permutation test Z-score values ~ 4.0), but node strength, eigencentrality, and clustering coefficients do show significant elevation ($p < 0.01$) in the high-gamma band. These three measures again appear strongly correlated as in the case for the corresponding AEC-based measures.

ROC analyses show that AEC-based graph metrics in the low-gamma band yield moderately high discriminability of the SOZ (highest mean AUC of ~ 0.73 for node strength). We postulated that despite robust elevations of these graph metrics at the SOZ nodes, their specificity for identifying SOZ nodes may be compromised by two factors: (a) elevated levels of these metrics in hyperexcitable cortex in the vicinity of the SOZ (but outside it), and (b) high-connectivity nodes belonging to functional brain networks. As commented on earlier, the SOZ is only an approximation of the EZ, the hypothetical generator of seizures[3]. The RZ is typically larger than the SOZ and is what ultimately determines seizure outcomes following surgery. Furthermore, cortical hyperexcitability related to the pathology of focal epilepsy is not always limited to the vicinity of the SOZ[21], nor are traditional biomarkers of hyperexcitability such as epileptic spikes and high-frequency oscillations always contained within the RZ even in patients with excellent seizure outcomes[14]. Our finding that SOZ false-positives from ROC analyses of AEC-based node strength, eigencentrality, and clustering coefficients fall disproportionately within the RZ is consistent with the notion of increased cortical hyperexcitability in the vicinity of the SOZ. Whether high-connectivity nodes belonging to functional brain networks may be contributing to SOZ false positives is not possible to determine from our data alone, but some evidence of this is suggested by correlations between high-gamma AEC connectivity and results of electrical stimulation mapping[69] and increased high-gamma synchrony between task-related areas noted using PLVs[70]. Conversely, our results point to the need for caution when using FC analyses to identify functional networks in the cortex.

Graph metrics estimated from different patients may not be directly comparable due to differences in the range of connectivity values, noisy or spurious connections, and differing numbers of nodes (intracranial recording sites). This can be a concern if pooling data from different patients is desirable, for instance, to train a machine learning algorithm. One approach that has been proposed to address some of these issues involves estimating Minimum Spanning Trees (MST) from the connectivity matrices before calculating graph measures[50,71]. In the gamma band, we found that within-subject rescaling the graph metrics calculated from raw connectivity matrices to a (0,1) range and ROC analysis on the pooled data yielded AUCs identical to the average AUCs of ROCs performed on untransformed metrics in individual patients. The effectiveness of this strategy for normalizing inter-patient differences in the magnitudes of graph metrics is suggested by the correlograms of the low-gamma band AECs graph metrics. Without rescaling, the graph metrics from individual patients are seen to separate, but with the rescaling, they do not (See Fig. S3 provided with Supplementary material online). Applying the Minimum Spanning Tree approach to our AEC connectivity data in the low-gamma band did not improve the discriminability of the SOZ nodes over simply rescaling the graph metrics to a (0,1) range.

There have been several prior studies of FC in patients with focal epilepsy to identify epileptogenic networks from interictal ECoG. Comparison of results across these studies is made challenging by differences in the choice of connectivity measures, whether they were applied to broad-band versus narrow-band signals, and the specific graph metrics examined. Results likely also depend on whether epileptic spikes and HFOs were excluded from the ECoG samples subjected to FC analysis, and whether any transformations or normalizations were applied to the FC matrices or derived graph metrics. Nevertheless, increased node strength within the SOZ has been reported based on connectivity derived from measures as diverse as directed transfer functions (DTFs)[33], nonlinear correlations[29], AECs, and PLV[72,73]. However, the strong frequency dependence of differences in node strength or connectivity values between the SOZ and non-SOZ nodes that we predict and observe has not been previously reported. Although not commented on, a frequency dependence of AECs estimated from interictal Stereo-EEG recordings is suggested in the data from a recent study where mean AEC values within the SOZ were noted to be most prominently increased relative to other areas in the gamma band[72]. Our findings are also consistent with another recent study which noted that in patients with good seizure outcomes, AECs estimated without excluding epileptic spikes (i.e., under conditions comparable to our patient cohort and ECoG samples) yielded moderately elevated node strengths in the low-gamma band alone[73].

In our results, node eigencentrality is highly correlated to both node-strength and clustering coefficients and the three metrics very likely provide mutually redundant information about cortical excitability. In one previous study, node eigencentrality derived from FC estimated using the weighted phase lag index (wPLI) was noted to be increased within the SOZ for the fast ripple band (> 250 Hz) when epochs containing epileptic spikes were included in the analysis but was lower when interictal HFOs were present[34]. Node eigencentrality derived from AECs has been examined by Li et al., but the focus was the evolution of the graph metric over the course of ictal events to better define the epileptogenic zones[74]. Another recent study reported that eigencentrality values derived from five different connectivity measures (Pearson correlation, coherence, phase-locking value, phase-lag index, and mutual information) calculated from broadband ECoG signals (1–119 Hz) were generally lower in the SOZ compared to other areas[31]. We believe that these inconsistent results only highlight the importance of performing a frequency-resolved analysis of FC since broadband ECoG signals likely represent the behavior of multiple systems and thus a mixture of effects. We found betweenness centrality derived from AECs to be significantly increased within the SOZ across the gamma band. This is consistent with an early study of ECoG FC in epilepsy a small sample of patients which reported that betweenness centrality derived from interictal

FC defined by directed transfer functions (DTFs) was elevated in the SOZ[32], and also a more recent study using AECs and PLVs applied to interictal Stereo-EEG data[72].

It is noteworthy that the elevations of graph metrics based on AECs that we find are statistically most robust in the low gamma band. Several lines of evidence suggest that mechanisms that generate low and high gamma band activity are different. Low gamma activity in the 30–60 Hz band likely arises from excitatory-inhibitory feedback loops mediated by inhibitory interneurons in the cortex in contrast to broadband high gamma activity in the 80–200 Hz range which may be more directly related to pyramidal cell action potentials[51,75–77]. It is conceivable that firing rate correlations related to cortical hyperexcitability are more pronounced among interneuron populations that support excitatory-inhibitory feedback loops. At least one microelectrode study has recently reported increased synchrony among the interneuron populations in the neocortex but not the pyramidal cells in the preictal period immediately before seizure onset[78].

One limitation of our study is that we restrict our patient cohort exclusively to patients who maintained Engel Class IA (seizure-free) outcomes for > 2 years after surgery. Compared to studies involving patients with mixed surgical outcomes, this feature of our dataset may have helped amplify both the contrast of graph metrics between SOZ and non-SOZ areas and their frequency dependence. However, this also prevents us from using FC-derived measures to predict surgical outcomes to further validate the metrics as candidate biomarkers of focal epilepsy. A further limitation of our study is that our data comprised of ECoG signals recorded from subdural grids and strip electrodes. Only three patients had hybrid depth electrodes implanted to sample the activity from the medial temporal regions. Over the last decade, most epilepsy surgery centers have switched to stereotactic implantation of depth electrode arrays for invasive EEG studies (Stereo-EEG). While we see no a priori reasons why our results would not be replicable using stereo-EEG data recorded from cortical contacts, this remains to be verified. Our study did not examine the effect of distance from the SOZ on FC and graph metrics, with our comparisons being between the SOZ and non-SOZ nodes (with RZ nodes excluded from the latter grouping). The presence of increased inhibition surrounding the EZ has been suggested by models of focal epilepsy such as the penicillin model and observations in human focal epilepsy[79,80]. Whether this is a sustained increase in inhibition (decreased excitability) or an increased magnitude of reactive inhibition is not clear. If it is a sustained inhibition, this decreased excitability could potentially decrease gamma band AEC values within the immediate periphery of the SOZ (just as increased excitability increases it). This could potentially increase the contrast between SOZ and non-SOZ areas. Finally, we did not explicitly exclude epochs with spikes and HFOs from our computations of AECs and PLVs. Our rationale for not excluding epochs containing interictal epileptic phenomena from the analysis was that this would markedly reduce the number of epochs available for analysis in each patient and introduce a source of large variability in the available number of epochs across patients, especially when HFOs are excluded. Some recent studies have noted more pronounced differences in AEC-derived graph metrics when epileptic spikes were retained while computing connectivity compared to when epochs containing epileptic spikes were excluded[72,73]. The key premise for this study is the notion that firing-rate correlations of neuronal populations in the interictal state are increased within hyperexcitable brain networks compared to normal brain areas. The term hyperexcitability has been used in the epilepsy literature to refer to both intrinsic irritability of the cortex as evidenced by interictal discharges or seizure initiation, as well as increased responsivity to excitatory afferent stimuli. Although paroxysmal epileptic phenomena such as interictal discharges or seizures have long been attributed to hypersynchronous neuronal activity within the epileptic cortex[40,41], single-cell studies have suggested a more complex and heterogeneous relationship between the firing rate synchrony of cells and synchronization of macroscopic signals such as EEG and local field potentials (LFPs), possibly due to limitations in adequately sampling large cell populations in the cortex as well as differences across various cell types[81]. In this paper, we use the term hyperexcitability to imply increased responsivity of the cortex due to elevated cortical gain or impaired gain control mechanisms. Hyperexcitability-related mutual excitation over short ranges could potentially increase correlations in the firing rates of neuronal populations within resting-state epileptic networks. This increased correlation of firing rates would be expected regardless of whether there are paroxysmal phenomena such as spikes, HFOs, or seizures. Nevertheless, without duplicating our analysis after excluding epochs containing HFOs and epileptic spikes it is difficult to say to what degree their presence might have contributed to the strongly elevated levels of AEC connectivity and related graph metrics that we find in the gamma band.

To summarize, we demonstrate that the magnitude of AECs estimated from interictal ECoG recordings shows strong frequency-dependent elevations within the epileptogenic cortex across the gamma frequency bands. AEC-based graph metrics also show statistically robust increases in the epileptogenic zones across the gamma band with maxima in the low-gamma band. These effects are consistent with an increase in firing-rate correlations among neuronal populations within the epileptogenic cortex, presumably related to cortical hyperexcitability. AEC-based node strength, eigencentrality, and clustering coefficient yield moderately high discriminability of the SOZ and may be potential surrogate markers of cortical hyperexcitability. These measures are also strongly correlated to each other and likely provide mutually redundant information. The degree to which high-connectivity nodes belonging to functional brain networks represent a potential confound remains to be determined. By contrast to AEC-based connectivity findings, we find that graph metrics derived from PLVs show modest alterations in the epileptogenic cortex, reaching statistical significance only in the high-gamma band. The relative simplicity of estimating gamma band AECs and node strengths makes them attractive benchmarks against which more sophisticated putative interictal biomarkers of cortical hyperexcitability may be readily compared. No one surrogate marker of cortical hyperexcitability will likely suffice to map the full extent of the epileptogenic network and it may be necessary to integrate information across multiple features including traditional features such as epileptic spikes and power spectral density using machine learning approaches[82,83].

Data availability

Detailed patient-wise demographic and clinical variables are provided in Table S1 (see Supplementary material online). Since this was a retrospective study, written informed consent for archived clinical data to be shared publicly was not available from our patient cohort. As such imaging and ECoG data for this study cannot be publicly shared. They may however be sought from the corresponding author (M.R., mraghavan@mmcw.edu) with the necessary deidentification, within the framework of a data-sharing agreement upon reasonable request.

Code availability

The scripts used for the analyses described in this manuscript are written in MATLAB (R2019b) and utilize display routines from EEG lab (https://sccn.ucsd.edu/eeglab/) and filtering routines from *FieldTrip* toolbox (https://www.fieldtriptoolbox.org/) which are both publicly available. Line noise removal during pre-processing of ECoG data was performed using publicly available code written by Calvin Eiber and Alexander Pietersen (2015) (Remove Line Noise: MATLAB Central File Exchange: https://www.mathworks.com/matlabcentral/fileexchange/54228-remove-line-noise). Graph metrics were calculated from functional connectivity matrices using the Brain Connectivity Toolbox which is openly available (https://sites.google.com/site/bctnet/). The MATLAB scripts used to calculate functional connectivity matrices from the ECoG data are available from the corresponding author upon reasonable request.

Received: 23 April 2024; Accepted: 8 July 2024
Published online: 31 July 2024

References

1. Spencer, S. S. Neural networks in human epilepsy: Evidence of and implications for treatment. *Epilepsia* **43**, 219–227 (2002).
2. Kwan, P. & Brodie, M. J. Early identification of refractory epilepsy. *N. Engl. J. Med.* **342**, 314–319 (2000).
3. Rosenow, F. & Lüders, H. Presurgical evaluation of epilepsy. *Brain* **124**, 1683–1700 (2001).
4. Lüders, H. O., Najm, I., Nair, D., Widdess-Walsh, P. & Bingman, W. The epileptogenic zone: General principles. *Epileptic Disorders* **8**, S1–S9 (2006).
5. Jehi, L. E., Silveira, D. C., Bingaman, W. & Najm, I. Temporal lobe epilepsy surgery failures: Predictors of seizure recurrence, yield of reevaluation, and outcome following reoperation. *J. Neurosurg.* **113**, 1186–1194 (2010).
6. Najm, I. *et al.* Temporal patterns and mechanisms of epilepsy surgery failure. *Epilepsia* **54**, 772–782 (2013).
7. Zijlmans, M., Zweiphenning, W. & van Klink, N. Changing concepts in presurgical assessment for epilepsy surgery. *Nat. Rev. Neurol.* **15**, 594–606 (2019).
8. Papadelis, C. & Perry, M. S. *Seminars in Pediatric Neurology*, Elsevier, 100919.
9. Bernabei, J. M. *et al.* Quantitative approaches to guide epilepsy surgery from intracranial EEG. *Brain* **146**, 2248–2258 (2023).
10. Badawy, R., Freestone, D., Lai, A. & Cook, M. Epilepsy: Ever-changing states of cortical excitability. *Neuroscience* **222**, 89–99 (2012).
11. Badawy, R. A., Curatolo, J. M., Newton, M., Berkovic, S. F. & Macdonell, R. A. Changes in cortical excitability differentiate generalized and focal epilepsy. *Ann. Neurol.* **61**, 324–331 (2007).
12. Porciatti, V., Bonanni, P., Fiorentini, A. & Guerrini, R. Lack of cortical contrast gain control in human photosensitive epilepsy. *Nat. Neurosci.* **3**, 259–263 (2000).
13. Frauscher, B. *et al.* High-frequency oscillations: the state of clinical research. *Epilepsia* **58**, 1316–1329 (2017).
14. Roehri, N. & Bartolomei, F. Are high-frequency oscillations better biomarkers of the epileptogenic zone than spikes?. *Curr. Opin. Neurol.* **32**, 213–219 (2019).
15. George, D. D., Ojemann, S. G., Drees, C. & Thompson, J. A. Stimulation mapping using stereoelectroencephalography: Current and future directions. *Front. Neurol.* **11**, 320 (2020).
16. Trébuchon, A. & Chauvel, P. Electrical stimulation for seizure induction and functional mapping in stereoelectroencephalography. *J. Clin. Neurophysiol.* **33**, 511–521 (2016).
17. Frauscher, B. *et al.* Stimulation to probe, excite, and inhibit the epileptic brain. *Epilepsia* **64**, S49 (2023).
18. Matsumoto, R., Kunieda, T. & Nair, D. Single pulse electrical stimulation to probe functional and pathological connectivity in epilepsy. *Seizure* **44**, 27–36 (2017).
19. Ramantani, G. *et al.* Passive and active markers of cortical excitability in epilepsy. *Epilepsia* **64**, S25 (2023).
20. Valentin, A. *et al.* Responses to single pulse electrical stimulation identify epileptogenesis in the human brain in vivo. *Brain* **125**, 1709–1718 (2002).
21. Badawy, R. A., Harvey, A. S. & Macdonell, R. A. Cortical hyperexcitability and epileptogenesis: Understanding the mechanisms of epilepsy-part 2. *J. Clin. Neurosci.* **16**, 485–500 (2009).
22. Badawy, R. A., Harvey, A. S. & Macdonell, R. A. Cortical hyperexcitability and epileptogenesis: Understanding the mechanisms of epilepsy–part 1. *J. Clin. Neurosci.* **16**, 355–365 (2009).
23. He, B. *et al.* Electrophysiological brain connectivity: Theory and implementation. *IEEE Trans. Biomed. Eng.* **66**, 2115–2137 (2019).
24. O'Neill, G. C. *et al.* Dynamics of large-scale electrophysiological networks: A technical review. *Neuroimage* **180**, 559–576 (2018).
25. Bastos, A. M. & Schoffelen, J.-M. A tutorial review of functional connectivity analysis methods and their interpretational pitfalls. *Front. Syst. Neurosci.* **9**, 175 (2016).
26. Lagarde, S., Bénar, C.-G., Wendling, F. & Bartolomei, F. Interictal functional connectivity in focal refractory epilepsies investigated by intracranial EEG. *Brain Conn.* **12**, 850–869 (2022).
27. Antony, A. R. *et al.* Functional connectivity estimated from intracranial EEG predicts surgical outcome in intractable temporal lobe epilepsy. *PloS One* **8**, e77916 (2013).
28. Jiang, H. *et al.* Interictal SEEG resting-state connectivity localizes the seizure onset zone and predicts seizure outcome. *Adv. Sci.* **9**, 2200887 (2022).
29. Lagarde, S. *et al.* Interictal stereotactic-EEG functional connectivity in refractory focal epilepsies. *Brain* **141**, 2966–2980 (2018).
30. Malladi, R., Kalamangalam, G., Tandon, N. & Aazhang, B. Identifying seizure onset zone from the causal connectivity inferred using directed information. *IEEE J. Select. Topics Signal Process.* **10**, 1267–1283 (2016).
31. Wang, A. *et al.* Resting-state SEEG-based brain network analysis for the detection of epileptic area. *J. Neurosci. Methods* **390**, 109839 (2023).
32. Wilke, C., Worrell, G. & He, B. Graph analysis of epileptogenic networks in human partial epilepsy. *Epilepsia* **52**, 84–93 (2011).
33. Zaveri, H. P. *et al.* Localization-related epilepsy exhibits significant connectivity away from the seizure-onset area. *Neuroreport* **20**, 891–895 (2009).
34. Zweiphenning, W. *et al.* High frequency oscillations and high frequency functional network characteristics in the intraoperative electrocorticogram in epilepsy. *NeuroImage Clin.* **12**, 928–939 (2016).

35. Mukamel, R. *et al.* Coupling between neuronal firing, field potentials, and FMRI in human auditory cortex. *Science* **309**, 951–954 (2005).
36. Mukamel, R. *et al.* Invariance of firing rate and field potential dynamics to stimulus modulation rate in human auditory cortex. *Human Brain Mapp.* **32**, 1181–1193 (2011).
37. Nir, Y. *et al.* Coupling between neuronal firing rate, gamma LFP, and BOLD fMRI is related to interneuronal correlations. *Curr. Biol.* **17**, 1275–1285 (2007).
38. Ray, S., Crone, N. E., Niebur, E., Franaszczuk, P. J. & Hsiao, S. S. Neural correlates of high-gamma oscillations (60–200 Hz) in macaque local field potentials and their potential implications in electrocorticography. *J. Neurosci.* **28**, 11526–11536 (2008).
39. Manning, J. R., Jacobs, J., Fried, I. & Kahana, M. J. Broadband shifts in local field potential power spectra are correlated with single-neuron spiking in humans. *J. Neurosci.* **29**, 13613–13620 (2009).
40. Margineanu, D. G. Epileptic hypersynchrony revisited. *Neuroreport* **21**, 963–967 (2010).
41. Penfield, W. & Jasper, H. Epilepsy and the functional anatomy of the human brain. (1954).
42. LaViolette, P. S. *et al.* Three-dimensional visualization of subdural electrodes for presurgical planning. *Neurosurgery* **68**, 152 (2011).
43. Mewett, D. T., Nazeran, H. & Reynolds, K. J. in *2001 conference proceedings of the 23rd annual international conference of the IEEE Engineering in Medicine and Biology Society.* 2190–2193 (IEEE).
44. Bruña, R., Maestú, F. & Pereda, E. Phase locking value revisited: Teaching new tricks to an old dog. *J. Neural Eng.* **15**, 056011 (2018).
45. Lachaux, J. P., Rodriguez, E., Martinerie, J. & Varela, F. J. Measuring phase synchrony in brain signals. *Human Brain Mapp.* **8**, 194–208 (1999).
46. Aydore, S., Pantazis, D. & Leahy, R. M. A note on the phase locking value and its properties. *Neuroimage* **74**, 231–244 (2013).
47. Mormann, F., Lehnertz, K., David, P. & Elger, C. E. Mean phase coherence as a measure for phase synchronization and its application to the EEG of epilepsy patients. *Phys. D Nonlinear Phenom.* **144**, 358–369 (2000).
48. García-Prieto, J., Bajo, R. & Pereda, E. Efficient computation of functional brain networks: Toward real-time functional connectivity. *Front. Neuroinf.* **11**, 8 (2017).
49. Rubinov, M. & Sporns, O. Complex network measures of brain connectivity: Uses and interpretations. *Neuroimage* **52**, 1059–1069 (2010).
50. Tewarie, P., van Dellen, E., Hillebrand, A. & Stam, C. J. The minimum spanning tree: An unbiased method for brain network analysis. *Neuroimage* **104**, 177–188 (2015).
51. Crone, N. E., Korzeniewska, A. & Franaszczuk, P. J. Cortical gamma responses: Searching high and low. *Int. J. Psychophysiol.* **79**, 9–15 (2011).
52. Crone, N. E. *et al.* Functional mapping of human sensorimotor cortex with electrocorticographic spectral analysis. I. Alpha and beta event-related desynchronization. *Brain J. Neurol.* **121**, 2271–2299 (1998).
53. Miller, K. J. *et al.* Spectral changes in cortical surface potentials during motor movement. *J. Neurosci.* **27**, 2424–2432 (2007).
54. Pfurtscheller, G. EEG event-related desynchronization (ERD) and synchronization (ERS). *Electroencephalograp. Clin. Neurophysiol.* **1**, 26 (1997).
55. Canolty, R. T. *et al.* High gamma power is phase-locked to theta oscillations in human neocortex. *Science* **313**, 1626–1628 (2006).
56. Canolty, R. T. & Knight, R. T. The functional role of cross-frequency coupling. *Trends Cognit. Sci.* **14**, 506–515 (2010).
57. Florin, E. & Baillet, S. The brain's resting-state activity is shaped by synchronized cross-frequency coupling of neural oscillations. *Neuroimage* **111**, 26–35 (2015).
58. Osipova, D., Hermes, D. & Jensen, O. Gamma power is phase-locked to posterior alpha activity. *PloS One* **3**, e3990 (2008).
59. Whittingstall, K. & Logothetis, N. K. Frequency-band coupling in surface EEG reflects spiking activity in monkey visual cortex. *Neuron* **64**, 281–289 (2009).
60. Voytek, B. *et al.* Shifts in gamma phase–amplitude coupling frequency from theta to alpha over posterior cortex during visual tasks. *Front. Human Neurosci.* **4**, 191 (2010).
61. Alper, K. *et al.* Localizing epileptogenic regions in partial epilepsy using three-dimensional statistical parametric maps of background EEG source spectra. *NeuroImage* **39**, 1257–1265 (2008).
62. Gallen, C. *et al.* Magnetic source imaging of abnormal low-frequency magnetic activity in presurgical evaluations of epilepsy. *Epilepsia* **38**, 452–460 (1997).
63. Ishibashi, H. *et al.* Detection and significance of focal, interictal, slow-wave activity visualized by magnetoencephalography for localization of a primary epileptogenic region. *J. Neurosurg.* **96**, 724–730 (2002).
64. Vanrumste, B., Jones, R. D., Bones, P. J. & Carroll, G. J. Slow-wave activity arising from the same area as epileptiform activity in the EEG of paediatric patients with focal epilepsy. *Clin. Neurophysiol.* **116**, 9–17 (2005).
65. Tao, J. X. *et al.* Interictal regional delta slowing is an EEG marker of epileptic network in temporal lobe epilepsy. *Epilepsia* **52**, 467–476 (2011).
66. Ali, R. *et al.* Phase-amplitude coupling measures for determination of the epileptic network: A methodological comparison. *J. Neurosci. Methods* **370**, 109484 (2022).
67. Hashimoto, H. *et al.* Phase-amplitude coupling between infraslow and high-frequency activities well discriminates between the preictal and interictal states. *Sci. Rep.* **11**, 17405 (2021).
68. Amiri, M., Frauscher, B. & Gotman, J. Phase-amplitude coupling is elevated in deep sleep and in the onset zone of focal epileptic seizures. *Front. Human Neurosci.* **10**, 387 (2016).
69. Ko, A. L., Weaver, K. E., Hakimian, S. & Ojemann, J. G. Identifying functional networks using endogenous connectivity in gamma band electrocorticography. *Brain Conn.* **3**, 491–502 (2013).
70. Arnulfo, G. *et al.* Long-range phase synchronization of high-frequency oscillations in human cortex. *Nature Commun.* **11**, 5363 (2020).
71. Stam, C. *et al.* The trees and the forest: characterization of complex brain networks with minimum spanning trees. *Int. J. Psychophysiol.* **92**, 129–138 (2014).
72. Corona, L. *et al.* Non-invasive mapping of epileptogenic networks predicts surgical outcome. *Brain* **146**, 1916–1931 (2023).
73. Rijal, S. *et al.* Functional connectivity discriminates epileptogenic states and predicts surgical outcome in children with drug resistant epilepsy. *Sci. Rep.* **13**, 9622 (2023).
74. Li, A. *et al.* Using network analysis to localize the epileptogenic zone from invasive EEG recordings in intractable focal epilepsy. *Netw. Neurosci.* **2**, 218–240 (2018).
75. Ray, S. & Maunsell, J. H. Different origins of gamma rhythm and high-gamma activity in macaque visual cortex. *PLoS Biol.* **9**, e1000610 (2011).
76. Ray, S. & Maunsell, J. H. Do gamma oscillations play a role in cerebral cortex?. *Trends Cogn. Sci.* **19**, 78–85 (2015).
77. Whittington, M. A., Cunningham, M. O., LeBeau, F. E., Racca, C. & Traub, R. D. Multiple origins of the cortical gamma rhythm. *Dev. Neurobiol.* **71**, 92–106 (2011).
78. Misra, A., Long, X., Sperling, M. R., Sharan, A. D. & Moxon, K. A. Increased neuronal synchrony prepares mesial temporal networks for seizures of neocortical origin. *Epilepsia* **59**, 636–649 (2018).
79. Serafini, R. & Loeb, J. A. Enhanced slow waves at the periphery of human epileptic foci. *Clin. Neurophysiol.* **126**, 1117–1123 (2015).
80. Trevelyan, A. J. & Schevon, C. A. How inhibition influences seizure propagation. *Neuropharmacology* **69**, 45–54 (2013).
81. Jiruska, P. *et al.* Synchronization and desynchronization in epilepsy: Controversies and hypotheses. *J. Physiol.* **591**, 787–797 (2013).

82. Cimbalnik, J. *et al.* Multi-feature localization of epileptic foci from interictal, intracranial EEG. *Clin. Neurophysiol.* **130**, 1945–1953 (2019).
83. Varatharajah, Y. *et al.* Integrating artificial intelligence with real-time intracranial EEG monitoring to automate interictal identification of seizure onset zones in focal epilepsy. *J. Neural Eng.* **15**, 046035 (2018).

Acknowledgements
We thank the Department of Neurology at the Medical College of Wisconsin, Milwaukee, Wisconsin for providing the computational resources for this project, and a gift from an anonymous donor that funded a graduate assistantship for JP over the duration of this study.

Author contributions
M.R., SB, and JP designed the study. M.R. retrieved and curated the clinical data, wrote the scripts for FC estimation, supervised data analysis, and drafted the manuscript. SB co-supervised the data analysis and contributed to manuscript preparation and revision. JP wrote scripts for additional analyses, performed the analysis, and contributed to manuscript preparation and revision. All other authors reviewed the results and contributed to critical revision of the manuscript and final approval.

Competing interests
The authors declare no competing interests.

Additional information
Supplementary Information The online version contains supplementary material available at https://doi.org/10.1038/s41598-024-67120-8.

Correspondence and requests for materials should be addressed to M.R.

Reprints and permissions information is available at www.nature.com/reprints.

Publisher's note Springer Nature remains neutral with regard to jurisdictional claims in published maps and institutional affiliations.